INORGANIC CHEMISTRY FRONTIERS

RESEARCH ARTICLE

View Article Online
View Journal | View Issue

Cite this: *Inorg. Chem. Front.*, 2023, **10**, 5602

The transformation of a zero-dimensional cluster into a one-dimensional chain structure achieving a dramatically enhanced birefringence in tin(II)-based oxalates†

Liying Ren,[a] Linhong Cheng,[a] Xiaoyan Zhou,[a] Jinxuan Ren,[a] Liling Cao, *[a] Ling Huang, [a] Xuehua Dong,[a] Yuqiao Zhou, [b] Daojiang Gao[a] and Guohong Zou *[b]

Received 29th June 2023,
Accepted 18th August 2023

DOI: 10.1039/d3qi01213a

rsc.li/frontiers-inorganic

Developing new birefringent materials with large optical anisotropy is extremely urgent due to the fantastic progress of laser science and technology. Here, two tin(II)-based oxalates, $K_2Sn(C_2O_4)_2{\cdot}H_2O$ and $K_2Sn_2(C_2O_4)_2F_2{\cdot}H_2O$, were successfully synthesized by simultaneously introducing π-conjugated $[C_2O_4]^{2-}$ groups and distorted Sn^{2+}-polyhedra with stereochemically active lone pairs. The use of F^- regulates the arrangement of birefringence-active groups, resulting in the transformation of zero-dimensional (0D) $K_2Sn(C_2O_4)_2{\cdot}H_2O$ into 1D $K_2Sn_2(C_2O_4)_2F_2{\cdot}H_2O$, which successfully enhances birefringence from 0.103@546 nm to 0.301@546 nm. Meaningfully, detailed structural and property analysis demonstrates that the ideal spatial arrangement of all the birefringence-active functional modules can induce strong optical anisotropy, providing an idea for designing birefringent materials with excellent properties.

Introduction

Birefringent crystals, an important component of optoelectronic devices, exhibit strong light modulation ability.[1,2] In particular, crystals with large birefringence play an extremely critical role in both military and civilian applications, such as medical diagnosis, fiber-optic communications, flat panel displays, polarimetry, *etc.*[3,4] In the past decades, many birefringent crystals, including natural (*e.g.*, quartz crystal, mica, calcite and so on) and artificial (*e.g.*, α-BaB_2O_4(α-BBO),[5] MgF_2,[6] YVO_4 [7] and so on) birefringent crystals, have been discovered and synthesized. Among these some have already gained commercial interest, but their inherent defects, such as unavoidable impurities of natural crystals and low transmittance in the UV region for YVO_4 [7] and $CaCO_3$,[8] prevent their application in more advanced miniature optical devices for future markets. Therefore, the pressing need for new optical crystals with excellent performance, a large birefringence, stable physicochemical properties and easy growth characteristics is driving research efforts.

The birefringence of crystals essentially arises from the anisotropic response of the electron distribution to the applied electric field, and the following groups have been confirmed to enhance the birefringence of compounds due to their strong anisotropic response: (1) π-conjugated planar units, such as H_xBO_3(x = 0–3), H_xCO_3(x = 0–2), $H_xB_3O_6$(x = 0–3), $H_xC_3N_3O_3$(x = 0–3), and $H_xC_3O_4$(x = 0–4).[9–17] Wang's group reported that $Rb_3Na(H_2C_3N_3O_3)_4{\cdot}3H_2O$[18] crystals exhibit a large birefringence of 0.368@1064 nm, which essentially derives from delocalized conjugated orbitals on the planar $(H_2C_3N_3O_3)^-$. (2) Distorted tetrahedral moieties, such as fluorooxoborates $[BO_xF_{4-x}]^{(x+1)-}$ and fluorophosphates PO_3F, which have produced $BaB_8O_{12}F_2$ (0.116@1064 nm)[19] and $(N_2H_6)[HPO_3F]_2$ (0.077@1064 nm)[20] with enhanced birefringence. (3) Jahn–Teller cations include the specifically octahedrally coordinated d^0 transition metals (TMs: Mo^{6+}, W^{6+}, V^{5+}, and Nb^{5+}) and cations with stereochemically active lone pairs (SCALP, I^{5+}, Te^{4+}, Se^{4+}, and Sn^{2+}) such as d^0 transition metal cations Nb^{5+} in $K_3Nb_3Ge_2O_{13}$ (0.196@546 nm)[21] and (*R*)- and (*S*)-$[C_8H_{10}NO_3]_2[NbOF_5]$ (0.19–0.199@589.3 nm),[22] Ti^{4+} in $BaTi(BO_3)_2$ (0.169@546 nm),[23] stereochemically active lone pair (SCALP) cations Sn^{2+} in Sn_2PO_4Br (0.336@546 nm),[24] Sb^{3+} in $K_2SbP_2O_7F$ (0.157@546 nm),[25] and SbB_3O_6 (0.290@546 nm),[26] I^{5+} in $LiGaF_2(IO_3)_2$ (0.206@532 nm).[27] The current strategy

[a]*College of Chemistry and Materials Science, Sichuan Normal University, Chengdu 610066, P. R. China. E-mail: llcao21@163.com*
[b]*College of Chemistry, Sichuan University, Chengdu 610065, P. R. china. E-mail: zough@scu.edu.cn*

†Electronic supplementary information (ESI) available: Additional crystallographic data, XRD patterns, IR spectra, TGA, the residue of TGA and UV-vis-NIR diffuse reflectance spectra of $K_2Sn(C_2O_4)_2{\cdot}H_2O$ and $K_2Sn_2(C_2O_4)_2F_2{\cdot}H_2O$. CCDC 2267040 for $K_2Sn(C_2O_4)_2{\cdot}H_2O$ and 2267041 for $K_2Sn_2(C_2O_4)_2F_2{\cdot}H_2O$. For ESI and crystallographic data in CIF or other electronic format see DOI: https://doi.org/10.1039/d3qi01213a

focuses on the simultaneous introduction of multiple birefringence-active functional modules (FMs) mentioned above into one structure to construct optical materials with large birefringence. Noteworthily, the large birefringence is determined not only by the screening of FMs, but also their spatial arrangement. In 2018, Jayakanth Ravichandran *et al.* found that the quasi-one-dimensional (quasi-1D) structural configuration in $BaTiS_3$ could increase the polarizability anisotropy and favorably bring large birefringence up to 0.76 in the mid- to long-wave infrared region.[28] Beyond that, the structural advantages of the 1D configuration are also reflected in Na_2BP_2 (0.68@2000 nm)[29] and $[C(NH_2)_3]Sb(C_2O_4)F_2{\cdot}H_2O$ (0.323@546 nm).[30] Hence, selecting suitable FMs to construct 1D structures is a promising strategy to gain crystals with large birefringence.

Obviously, a 1D configuration is an ideal structural framework for obtaining large birefringence as described above. Nevertheless, not all birefringence-active FMs can be constructed into chains, since the formation of chains has an indispensable condition, *i.e.*, FMs with a unique coordination environment can prevent chain-to-chain connection and extension. So how do we effectively screen out the appropriate birefringence-active FMs? In molecular engineering, chemical scissors have been proved to be reliable structure-directing agents in the controlled design of crystal microstructures. To our knowledge, lone pair electrons act as chemical scissors to architecturally shape the target structure in many classical compounds of Pb_2BO_3Cl,[31] $Cs_2Pb(NO_3)_2Br_2$,[32] and $KSb_2C_2O_4F_5$,[33] because cations occupied by lone pair electrons on one side can form highly distorted polyhedra that not only exhibit large anisotropic polarizabilities, but also prevent connection with other structure modules on the same side. The Sn^{2+} cation is a highly promising candidate that, in addition to possessing SCALP, has rich coordination modes (terdentate, quadridentate, quinquidentate, and sexadentate),[34–36] allowing for increased structural diversity, *e.g.*, $Sn_2B_5O_9Cl$,[37] α-SnF_2,[38] $K_3Sn_2(SO_4)_3Cl$,[34] and $Sn_2[B_7O_{12}]F$.[39] In addition, the presence of planar anionic groups is essential for the development of low-dimensional structures because of their unique structural malleability. In recent years, experimental and theoretical evidence from Pan's and Zou's groups has demonstrated that planar $C_2O_4^{2-}$ groups are promising birefringence-active FMs, as exemplified by $(NH_4)_2C_2O_4{\cdot}H_2O$,[40] $Na_2Sb_2(C_2O_4)F_6$,[41] $Cs_2Sb_2(C_2O_4)_2F_4{\cdot}H_2O$ [41] and so on. The four O atoms of the $C_2O_4^{2-}$ groups all lie in the same plane, resulting in adjacent groups extending along the plane by sharing O atoms and ultimately forming a low-dimensional structure. In terms of properties, the $C_2O_4^{2-}$ groups exhibit strong π-conjugated interactions due to shorter bond lengths, strong P_π–P_π interactions and additional electron-populated p orbitals provided by C and O atoms, resulting in the production of large anisotropic polarizability and even large birefringence.

Based on the above ideas, the Sn^{2+}–$C_2O_4^{2-}$ system has been studied systematically. $K_2Sn(C_2O_4)_2{\cdot}H_2O$ was successfully synthesized by the hydrothermal reaction method. Regrettably, however, although $K_2Sn(C_2O_4)_2{\cdot}H_2O$ consists of Sn^{2+}-polyhedra and $C_2O_4^{2-}$ groups, it features a 0D anionic structure. We noticed that F^- ions are also widely considered to be excellent chemical scissors. When the F^- ions are introduced into the cation-centered polyhedra(M-polyhedra) of oxygenates, the other oxygen ligands are squeezed and moved toward the equator, which not only decrease the symmetry of the polyhedra, but also facilitate the extension of the polyhedra by sharing oxygen atoms. The C–F bond, which is generally shorter than the M–O bond, could cut the connecting bridge of chain to chain. As a result, F^- was considered for introduction into the Sn^{2+}–$C_2O_4^{2-}$ system, and $K_2Sn_2(C_2O_4)_2F_2{\cdot}H_2O$ featuring a unique 1D anionic structure was successfully synthesized by the solution evaporation method. Fascinatingly, as the crystal structure transforms from 0D to 1D, the birefringence increases dramatically from 0.103@546 nm in $K_2Sn(C_2O_4)_2{\cdot}H_2O$ to 0.301@546 nm as expected.

Experimental section

Synthesis of $K_2Sn(C_2O_4)_2{\cdot}H_2O$ and $K_2Sn_2(C_2O_4)_2F_2{\cdot}H_2O$

Reaction reagents: SnO (AR, 99%), $K_2C_2O_4{\cdot}H_2O$ (AR, 99.8%), SnF_2 (AR, 99%), and HF (AR, ≥40.0%). All materials were used as received and without further operation. There are some important things to follow when using HF: pay attention to ventilation, do a good job of safety protection, wear rubber acid-alkali resistant clothing and gloves, wash your hands thoroughly after use, and keep the place clean.

The compound $K_2Sn(C_2O_4)_2{\cdot}H_2O$ was synthesized by the hydrothermal reaction method. SnO (0.135 g) and $K_2C_2O_4{\cdot}H_2O$ (0.737 g) were added into H_2O (3 mL) and HF (0.1 mL). After 20 minutes of stirring, the mixture was sealed into an autoclave with a 23 mL Teflon liner and heated at 100 °C for 5 days, and then slowly cooled down to room temperature at 6 °C h^{-1}. In order to obtain a pure compound, the reaction mixture has to be rinsed with ethanol, and dried in air.

The compound $K_2Sn_2(C_2O_4)_2F_2{\cdot}H_2O$ was gained by the solution evaporation method. A mixture of SnF_2 (0.317 g) and $K_2C_2O_4{\cdot}H_2O$ (0.252 g) with a molar ratio of 2 : 3 was dissolved in H_2O (5 mL), and the solution was reddish brown after stirring for 20 minutes. Then the solution was transferred into a refrigerator at 4 °C. After 5 days, the reaction product was washed with ethanol and dried in air. Finally, block-like crystals were obtained.

Single crystal structure determination

By using a Rigaku XtaLAB Synergy R diffractometer with graphite monochromatic Mo-Kα radiation, the single crystal data of $K_2Sn(C_2O_4)_2{\cdot}H_2O$ and $K_2Sn_2(C_2O_4)_2F_2{\cdot}H_2O$ can be obtained at 150(2) K. The structures of the two compounds were refined with SHELXL-2014.[42] We used the program PLATON[43] to inspect the structure, and no higher symmetries could be found. The related crystal data and structure refinement of the two compounds are listed in Tables S1–S5.†

Powder X-ray Diffraction

A SmartLab powder X-ray diffractometer with Cu-Kα radiation was used to gather the powder X-ray diffraction patterns for $K_2Sn(C_2O_4)_2{\cdot}H_2O$, and $K_2Sn_2(C_2O_4)_2F_2{\cdot}H_2O$ at room temperature. The decay test conditions are as follows: the 2θ angular range starts from 5° and stops at 70°, the scan step width is 0.02°, and the fixed time is 0.2 s. The test results show that the experimental pattern is consistent with the calculated pattern (Fig. S1†).

Thermal analysis

Thermogravimetric analysis of the two compounds was performed using NETZSCH STA-449C with a constant flow of N_2 gas and the test temperature was from room temperature to 800 °C, with a heating rate of 10 °C per min (Fig. S2†).

Infrared spectroscopy

The data of infrared (IR) spectroscopy for $K_2Sn(C_2O_4)_2{\cdot}H_2O$ and $K_2Sn_2(C_2O_4)_2F_2{\cdot}H_2O$ were recorded with a Fourier transform infrared (FTIR) spectrometer with the model number Vertex 70. The range of measurement is 4000–400 cm^{-1}. The proportion of the sample and dried KBr is about 1 : 100 (Fig. S4†).

UV–Vis diffuse reflectance spectroscopy

A Shimadzu UV-2600 spectrophotometer was used to record the data of UV-vis diffuse reflectance spectroscopy for the two compounds with the wavelength range of 200–800 nm at room temperature (Fig. S5†).

Birefringence measurements

Birefringence tests of $K_2Sn(C_2O_4)_2{\cdot}H_2O$ and $K_2Sn_2(C_2O_4)_2F_2{\cdot}H_2O$ were conducted on a ZEISS Axio Scope A5 polarizing microscope with a Berek compensator. The formula used to calculate the birefringence is listed as follows:

$$\Delta R = \Delta n \times d. \quad (1)$$

ΔR indicates the optical path difference, Δn refers to the birefringence, and d is the thickness of the crystal. The results of the tests are shown in Fig. S6.†

Theoretical calculations

The data of the theoretical calculations for both the compounds were calculated using a Cambridge Serial Total Energy Package (CASTEP)[44] program, which is based on density functional theory (DFT).[45] In this way, we could calculate the band structure, density of states, optical properties and so on. The Perdew–Burke–Ernzerhof (PBE)[46] functional with Generalized Gradient Approximation (GGA) was employed for all calculations. To simplify the potential energy of all the atoms, Norm-conserving Pseudopotential (NCP)[47] was adopted. The kinetic energy cutoffs for $K_2Sn(C_2O_4)_2{\cdot}H_2O$ and $K_2Sn_2(C_2O_4)_2F_2{\cdot}H_2O$ were 750 eV, and the k-points in the first Brillouin zone were 4 × 4 × 2 ($K_2Sn(C_2O_4)_2{\cdot}H_2O$) and 2 × 3 × 2 ($K_2Sn_2(C_2O_4)_2F_2{\cdot}H_2O$). The valences of all atoms are listed below: H $1s^1$, C $2s^22p^2$, O $2s^22p^4$, F $2s^22p^5$, K $3s^23p^64s^1$, Sn $4d^{10}5s^25p^2$.

Results and discussion

Crystal structures

The two centrosymmetric Sn^{2+}-based oxalates $K_2Sn(C_2O_4)_2{\cdot}H_2O$ and $K_2Sn_2(C_2O_4)_2F_2{\cdot}H_2O$ crystallize in the triclinic space group $P\bar{1}$(No. 2) and $P2_1/c$ (No. 14), respectively, and the crystal structure of $K_2Sn(C_2O_4)_2{\cdot}H_2O$[48] was previously reported. Their basic functional anionic groups are planar π-conjugated $[C_2O_4]^{2-}$ with rational bond lengths (C–O: 1.228–1.286 Å and C–C: 1.550–1.558 Å) and bond angles (O–C–O: 123.7–126.7°, O–C–C: 115.4–120.3°), which are interconnected with the cationic building modules Sn^{2+}-based polyhedra and K^+ cations to assemble crystal frameworks respectively (Fig. 1). It is interesting that the diverse coordination environments and spatial arrangements in these building blocks lead to the unique crystal structures of these two compounds.

$K_2Sn(C_2O_4)_2{\cdot}H_2O$ contains one independent Sn atom, two K atoms, four C atoms, and nine O atoms in a unit cell. The Sn atom is four coordinated with four O atoms to form a SnO_4 seesaw polyhedron with Sn–O bond distances of 2.148–2.375 Å (Fig. 1a). Each SnO_4 seesaw polyhedron is linked to two nearly perpendicular $[C_2O_4]^{2-}$ planar groups by sharing four O atoms to form a 0D $[Sn(C_2O_4)_2]^{2-}$ anionic structure (Fig. 1b). In addition, K^+ cations with charge compensation and H_2O molecules are distributed in the voids of these $[Sn(C_2O_4)_2]^{2-}$ clusters (Fig. 1c).

For the compound $K_2Sn_2(C_2O_4)_2F_2{\cdot}H_2O$, the two independent Sn1 and Sn2 atoms are all connected with four O atoms and one F atom in a SnO_4F tetragonal pyramid with the bond length of Sn–O of 2.281–2.729 Å and that of Sn–F of 2.020–2.045 Å, respectively (Fig. 1d). The $[C_2O_4]^{2-}$ planar groups act as bridges to connect $[Sn(1)O_4F]^{7-}$ and $[Sn(2)O_4F]^{7-}$ in opposite directions by sharing O atoms, constructing a 1D $[Sn_2(C_2O_4)_2F_2]_\infty^{2-}$ anionic structure, and these chains are parallel to each other. The K atoms and H_2O molecules are arranged between the chains, with the K atoms playing a major role in charge-balancing (Fig. 1e and f).

Thermal analysis

The results of thermogravimetric analysis of the two title compounds are shown in Fig. S2.† The decomposition temperatures of $K_2Sn(C_2O_4)_2{\cdot}H_2O$ and $K_2Sn_2(C_2O_4)_2F_2{\cdot}H_2O$ are 40 °C and 42 °C, and the corresponding total weight loss rates are about 40% and 27%, respectively. The final decomposition products of these two compounds were tested by X-ray powder diffraction, demonstrating that the main products of the two compounds are SnO_2 and K_2SnO_3 in $K_2Sn(C_2O_4)_2{\cdot}H_2O$ and SnO_2 in $K_2Sn_2(C_2O_4)_2F_2{\cdot}H_2O$, respectively (Fig. S3†).

Infrared spectroscopy

As shown in Fig. S4,† the IR spectra of $K_2Sn(C_2O_4)_2{\cdot}H_2O$ and $K_2Sn_2(C_2O_4)_2F_2{\cdot}H_2O$ were recorded from 4000 to 400 cm^{-1}. The

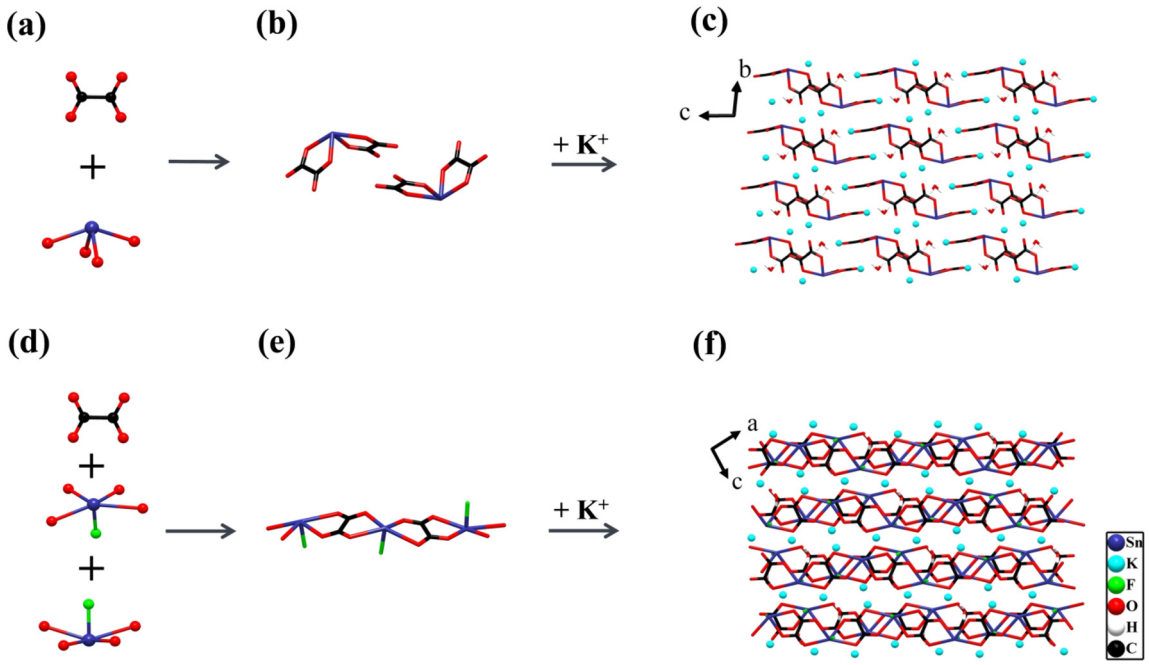

Fig. 1 (a and d) The coordination modes of Sn^{2+} and planar $[C_2O_4]^{2-}$ groups; (b and e) the different connection modes between Sn^{2+}-polyhedra and $[C_2O_4]^{2-}$ groups; (c and f) the structure of $K_2Sn(C_2O_4)_2{\cdot}H_2O$ and $K_2Sn_2(C_2O_4)_2F_2{\cdot}H_2O$ along the *a*-axis and *b*-axis, respectively.

peaks from 3416 cm^{-1} to 3709 cm^{-1} are the stretching vibrations of H_2O. The peaks at 1637 cm^{-1} and 1642 cm^{-1} are identified as the stretching vibrations of C=O bonds. The bands at 1485 cm^{-1}, 1421 cm^{-1}, 1273 cm^{-1}, and 1047 cm^{-1} can be ascribed to C–O stretching vibrations. The peaks at about 887 cm^{-1}, 783 cm^{-1} and 786 cm^{-1} are considered to be the stretching vibrations of C–C and bending vibrations of O–C=O bonds. The characteristic absorption bands at around 493 cm^{-1} and 487 cm^{-1} belong to the vibrations of Sn–F bonds for $K_2Sn_2(C_2O_4)_2F_2{\cdot}H_2O$. All of the vibrations are in agreement with previously reported spectra in the literature.[18,41,49–51]

UV–Vis diffuse reflectance spectroscopy

The UV-vis diffuse reflectance spectra of $K_2Sn(C_2O_4)_2{\cdot}H_2O$ and $K_2Sn_2(C_2O_4)_2F_2{\cdot}H_2O$ are shown in Fig. S5.† It reveals that the band gaps of $K_2Sn(C_2O_4)_2{\cdot}H_2O$ and $K_2Sn_2(C_2O_4)_2F_2{\cdot}H_2O$ are 3.74 eV and 3.21 eV, and the corresponding UV absorption cutoff edges are 286 nm and 310 nm, respectively, illustrating that the two compounds can be used in the ultraviolet region.

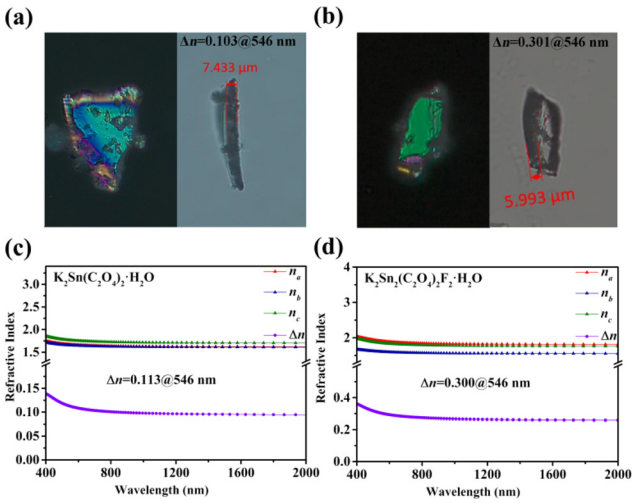

Fig. 2 (a and b) Experimental birefringence at 546 nm; (c and d) calculated refractive index for $K_2Sn(C_2O_4)_2{\cdot}H_2O$ and $K_2Sn_2(C_2O_4)_2F_2{\cdot}H_2O$.

Birefringence measurements

A ZEISS Axio A5 polarizing microscope was used to measure the birefringence of $K_2Sn(C_2O_4)_2{\cdot}H_2O$ and $K_2Sn_2(C_2O_4)_2F_2{\cdot}H_2O$ at 546 nm. The retardation and thickness of these two are 762 nm, 1803 nm and 7.433 μm, 5.993 μm, respectively. After substituting these values into eqn (1), the birefringence values of $K_2Sn(C_2O_4)_2{\cdot}H_2O$ and $K_2Sn_2(C_2O_4)_2F_2{\cdot}H_2O$ were obtained as 0.103 and 0.301 at 546 nm, respectively (Fig. 2a and b). In addition, the refractive indices of the compounds are calculated and presented in Fig. 2c and d. The results show that $K_2Sn(C_2O_4)_2{\cdot}H_2O$ is positive biaxial crystals ($n_z - n_y > n_y - n_x$) and $K_2Sn_2(C_2O_4)_2F_2{\cdot}H_2O$ is negative biaxial crystals ($n_z - n_y < n_y - n_x$). The calculated birefringence of these compounds is 0.113 and 0.300 at 546 nm, respectively, which closely match the experimental values. It is obvious that $K_2Sn_2(C_2O_4)_2F_2{\cdot}H_2O$ has a significantly enhanced birefringence compared to $K_2Sn(C_2O_4)_2{\cdot}H_2O$, which surpasses that of traditional birefringent crystals such as $LiNbO_3$ (0.074@546 nm),[52] MgF_2 (0.012@532 nm),[6] α-BBO (0.122@546 nm),[5] $CaCO_3$ (0.172@532 nm),[8] YVO_4 (0.204@532 nm),[7] and TiO_2

(0.256@546 nm),[53] and some reported oxalate crystals, *e.g.*, $(CN_4H_7)SbC_2O_4F_2(H_2O)_{0.5}$ (0.126@546 nm),[54] $KSb_2C_2O_4F_5$ (0.170@546 nm),[33] $Rb_2C_2O_4$ (0.201@1064 nm),[55] and $(NH_4)_2SbC_2O_4Cl_3$ (0.270@546 nm).[56] Besides, the title compounds are preferred in terms of stable physicochemical properties, suggesting that Sn^{2+}-oxalates can be used as potential birefringent materials.

Molecular engineering regulates birefringence

As described above, these two compounds employ the same birefringence-active FMs, *i.e.*, π-conjugated $[C_2O_4]^{2-}$ planar groups and Sn^{2+} cations with SCALP, but their birefringence changes tremendously, which may indicate that the spatial arrangement of the FMs has a significant effect on the birefringence. By comparing the structural features of the two compounds, the only difference lies in the construction of the FMs, namely a 0D $[Sn(C_2O_4)_2]^{2-}$ anionic structure in $K_2Sn(C_2O_4)_2{\cdot}H_2O$ and a 1D $[Sn_2(C_2O_4)_2F_2]_\infty^{2-}$ anionic structure in $K_2Sn_2(C_2O_4)_2F_2{\cdot}H_2O$. Then, the spatial arrangement characteristics of these two are analyzed in detail. The lone pair electrons of the Sn^{2+} cation act as chemical scissors to shear the tendency to connect to its ipsilateral side, so that all O ligands of the Sn are evenly distributed on the other side of the lone pair electrons in $K_2Sn(C_2O_4)_2{\cdot}H_2O$. As a result, the $[C_2O_4]^{2-}$ groups connected to the SnO_4 seesaw polyhedron by shared O atoms are arranged non-coplanarly, and inconsistent orientations between $[C_2O_4]^{2-}$ groups and lone pair elections lead to a moderate birefringence of 0.103@546 nm (Fig. 3a and b). $K_2Sn_2(C_2O_4)_2F_2{\cdot}H_2O$ has not only the chemical scissors of the lone pair electrons, but also other chemical scissors of the fluorine atoms. The shorter Sn–F bonds keep the chain from being linked to another chain by sharing F atoms in one direction, successfully forming the $[Sn_2(C_2O_4)_2F_2]_\infty^{2-}$ chains in $K_2Sn_2(C_2O_4)_2F_2{\cdot}H_2O$. The 1D anionic structure is widely recognized as a structural mode with great potential to produce large birefringence, such as $Na_2Sb_2(C_2O_4)F_6$ and $Cs_2Sb_2(C_2O_4)_2F_4{\cdot}H_2O$. In addition, the introduced F ligand occupies the space around Sn^{2+}, forcing the four O ligands to shift toward the equatorial position of the Sn atom. Naturally, the $[C_2O_4]^{2-}$ groups attached to the Sn^{2+}-polyhedra also tend to be arranged in parallel, further enabling effective superposition of π-conjugated orbitals. In $K_2Sn_2(C_2O_4)_2F_2{\cdot}H_2O$, there is only one wave-like $[Sn_2(C_2O_4)_2F_2]_\infty^{2-}$ chain consisting of alternating linkages of a SnO_4F tetragonal pyramid and $[C_2O_4]^{2-}$ groups named chain A. As expected, all the $[C_2O_4]^{2-}$ groups in one chain are arranged with near coplanarity, and all of the SnO_4F tetragonal pyramids stand neatly. Subsequently, all chains A are arranged strictly parallel in the *ac* plane (Fig. 3c and d), with the lone pair electrons of Sn^{2+} and the π-conjugated electrons of the $[C_2O_4]^{2-}$ group lying in the same plane. Such a regular planar arrangement and uniform orientation result in $K_2Sn_2(C_2O_4)_2F_2{\cdot}H_2O$ exhibiting a large birefringence of 0.301@546 nm, which is approximately 2.9 times larger than that of $K_2Sn(C_2O_4)_2{\cdot}H_2O$. Thus, achieving a parallel and consistent alignment of birefringence-active FMs may be an effective approach to obtain significantly enhanced birefringence.

In this work, synergetic interactions of Sn^{2+} cations with SCALP and π-conjugated $[C_2O_4]^{2-}$ anion groups makes the birefringence vary dramatically from 0.103@546 nm of $K_2Sn(C_2O_4)_2{\cdot}H_2O$ to 0.301@546 nm of $K_2Sn_2(C_2O_4)_2F_2{\cdot}H_2O$ based on the structure–property relationship. To investigate in depth the contribution of birefringence-active FMs to the birefringence of the compounds, a detailed analysis of the microscopic mechanism is further conducted. First, the optical properties of all FMs were calculated using the Gaussian 09 package. As shown in Fig. 4a, the results indicate that the polarization anisotropy of the SnO_4F tetragonal pyramid is significantly greater than that of the SnO_4 seesaw polyhedron as expected. For $[C_2O_4]^{2-}$ groups with slight flexibility, the dihedral angles between the two $[CO_2]$ in one $[C_2O_4]^{2-}$ group range from 1.512° to 6.736° in the title compounds. Therefore, the small degree of distortion of $[C_2O_4]^{2-}$ groups has a negligible effect on their optical anisotropy (Table S6†). Obviously, the individual birefringence-active FM with superior polarization anisotropy is not the only essential factor to obtain a large birefringence, since birefringence originates from the effective superposition of microscopic polarization anisotropies of all birefringence-active FMs, which is reflected in their spatial orientation and density. In this work, the calculated refractive index shows that the two compounds are biaxial crystals, and the birefringence can be obtained by $\Delta n = n_z - n_x$. It can be speculated that the larger the birefringence-active FMs acting on the optical principal axis *Z* or the smaller on the *X*-axis, the more favorable it is to obtain a large birefringence. Therefore, the relationship between the *YZ* plane (*ac* plane for $K_2Sn(C_2O_4)_2{\cdot}H_2O$, *ac* plane for $K_2Sn_2(C_2O_4)_2F_2{\cdot}H_2O$) and the orientation of the lone pair electrons in the Sn^{2+} cations and the $C_2O_4^{2-}$ planes, respectively, is essential for exploring their contribution to birefringence. In Sn^{2+} cations with a SCALP, the lone pair electron is located on the opposite sides of the vector sum of the all Sn–O and/or Sn–F bonds of Sn^{2+}-based polyhedra, and the angle it forms with the *YZ* plane is defined as *α*. Ideally, the lone pair electron would make the largest con-

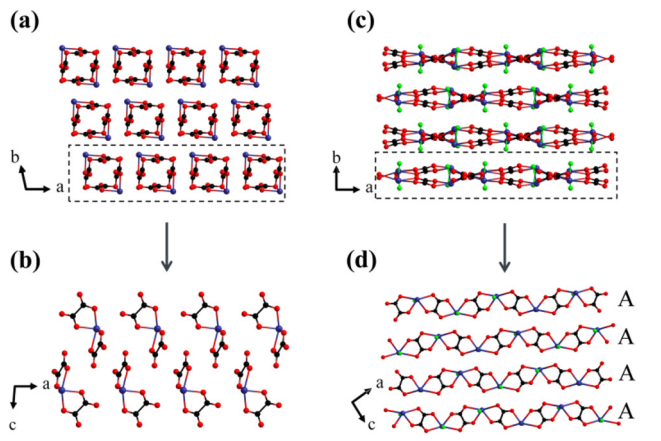

Fig. 3 The different arrangements of Sn^{2+}-$[C_2O_4]^{2-}$ groups in $K_2Sn(C_2O_4)_2{\cdot}H_2O$ (a and b) and $K_2Sn_2(C_2O_4)_2F_2{\cdot}H_2O$ (c and d).

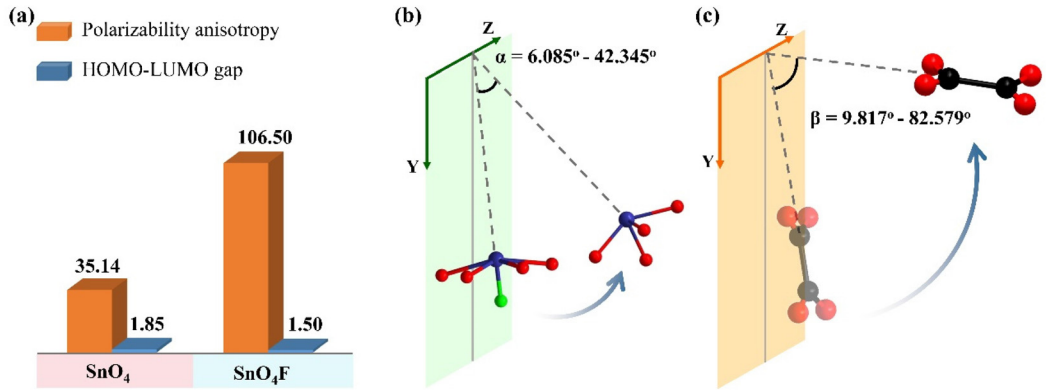

Fig. 4 (a) The polarizability anisotropy and HOMO–LUMO gap of Sn^{2+}-polyhedra (SnO_4 for $K_2Sn(C_2O_4)_2{\cdot}H_2O$ and SnO_4F for $K_2Sn_2(C_2O_4)_2F_2{\cdot}H_2O$); (b) the angles between the lone pair electron of Sn^{2+} and the *YZ* plane; and (c) the dihedral angles between the $[C_2O_4]^{2-}$ plane and *YZ* plane in $K_2Sn(C_2O_4)_2{\cdot}H_2O$ and $K_2Sn_2(C_2O_4)_2F_2{\cdot}H_2O$.

tribution to the birefringence when α is equal to 0°, *i.e.*, the lone pair electron is completely parallel to the *YZ* plane. Here, the $\cos\alpha$ values reveal that the contribution of the SnO_4 seesaw polyhedron in $K_2Sn(C_2O_4)_2{\cdot}H_2O$ to birefringence is significantly smaller than that of the SnO_4F tetragonal pyramid in $K_2Sn_2(C_2O_4)_2F_2{\cdot}H_2O$ (Fig. 4b) (Table S7†). In $C_2O_4^{2-}$ groups, the π-conjugated electrons that delocalized over the group plane are substantially responsible for the optical properties, so the anisotropic polarizability is very weak in the out-of-plane direction, especially perpendicular to the $C_2O_4^{2-}$ plane, and strong in the plane direction. Subsequently, the β is adopted to describe the dihedral angle between the $C_2O_4^{2-}$ plane and the *YZ* plane, which varies abundantly in the two compounds. According to the $\cos\beta$ values of the two compounds in Fig. 4c, Table S7,† the order of contribution of $C_2O_4^{2-}$ groups to birefringence is completely the same as that of Sn^{2+}-polyhedra. Further considering the density of birefringence-active FMs in a unit cell, the contributions of π-conjugated $C_2O_4^{2-}$ anion groups and Sn^{2+}-based polyhedra with SCALP to birefringence exhibit corresponding increasing trends of 0.0047 < 0.0066 and 0.0030 < 0.0067 in $K_2Sn(C_2O_4)_2{\cdot}H_2O$ and $K_2Sn_2(C_2O_4)_2F_2{\cdot}H_2O$, respectively. Unsurprisingly, the result confirms the previous conclusion that the contribution from the $C_2O_4^{2-}$ anion groups and Sn^{2+}-polyhedra is almost equally responsible for the birefringence of the compounds. Furthermore, the result is consistent with $K_2Sn_2(C_2O_4)_2F_2{\cdot}H_2O$ having a large birefringence, followed by $K_2Sn(C_2O_4)_2{\cdot}H_2O$. Thus, the relationship between birefringence and the spatial arrangement of FMs in this work provides an idea to predict the birefringence of compounds containing lone pair electrons and/or π-conjugated planar groups.

Theoretical calculations

In order to further understand the structure–property relationship of $K_2Sn(C_2O_4)_2{\cdot}H_2O$ and $K_2Sn_2(C_2O_4)_2F_2{\cdot}H_2O$, the electronic band structure, total and partial density of states (DOS) and electronic density differences were calculated based on the DFT method. The calculated band gaps for $K_2Sn(C_2O_4)_2{\cdot}H_2O$ and $K_2Sn_2(C_2O_4)_2F_2{\cdot}H_2O$ are 3.00 eV and 2.29 eV, which are 0.74 eV, and 0.92 eV smaller than the experimental results, respectively (Fig. 5a and d). The reason for the underestimation of the calculated value is usually attributed to the utilization of the DFT-GGA method.[57]

The data of Total Density of States (TDOS) and Partial Density of States (PDOS) for the two title compounds in Fig. 5b and e can prove the contributions of atomic orbitals to the bands. For the valence band (VB) from −10 eV to the Fermi level, the contributions are attributed to the H-1s, C-2s, C-2p, O-2s, O-2p, K-4p, Sn-5s, and Sn-5p states in $K_2Sn(C_2O_4)_2{\cdot}H_2O$ and the H-1s, C-2s, C-2p, O-2s, O-2p, F-2p, K-4p, Sn-5s, and Sn-5p states are the main contributors in $K_2Sn_2(C_2O_4)_2F_2{\cdot}H_2O$. For the conduction band (CB), the H-1s, C-2s, C-2p, O-2p, K-4s, K-4p, Sn-5s, and Sn-5p states are the main contributors in $K_2Sn(C_2O_4)_2{\cdot}H_2O$ and $K_2Sn_2(C_2O_4)_2F_2{\cdot}H_2O$. In partial DOS, for $K_2Sn(C_2O_4)_2{\cdot}H_2O$, it is clearly known that there are overlaps between C-2s, C-2p, Sn-5s, and Sn-5p states and O-2s and O-2p states, indicating the presence of C–O and Sn–O covalent bonds in this compound. For $K_2Sn_2(C_2O_4)_2F_2{\cdot}H_2O$, the C-2s, C-2p, Sn-5s, and Sn-5p states overlap with the O-2s, O-2p, and F-2p states, illustrating the presence of C–O, Sn–O, and Sn–F covalent bonds in these compounds. For the two compounds, it is quite clear that the electron orbitals near the Fermi level are composed of C-2s, C-2p, Sn-5s, Sn-5p, O-2p ($K_2Sn(C_2O_4)_2{\cdot}H_2O$), C-2s, C-2p, Sn-5s, Sn-5p, O-2p, and F-2p ($K_2Sn_2(C_2O_4)_2F_2{\cdot}H_2O$), respectively. This shows that the linear optical properties of the two compounds are mainly derived from the synergy of the $C_2O_4^{2-}$ group and Sn^{2+}-based polyhedra. Furthermore, in comparison with $K_2Sn(C_2O_4)_2{\cdot}H_2O$, the birefringence can be further enhanced due to the neat arrangement of the 1D $[Sn_2(C_2O_4)_2F_2]_\infty^{2-}$ anionic structure caused by the scissor effect of the F atom with greater electronegativity in $K_2Sn_2(C_2O_4)_2F_2{\cdot}H_2O$. In the electron density difference maps of the two compounds (Fig. 5c and f), red electronic clouds are observed around the Sn^{2+} cations and $C_2O_4^{2-}$ planar groups, indicating that the lone pair electrons are stereoactive in Sn^{2+}-polyhedra and the strong interaction between C and O atoms

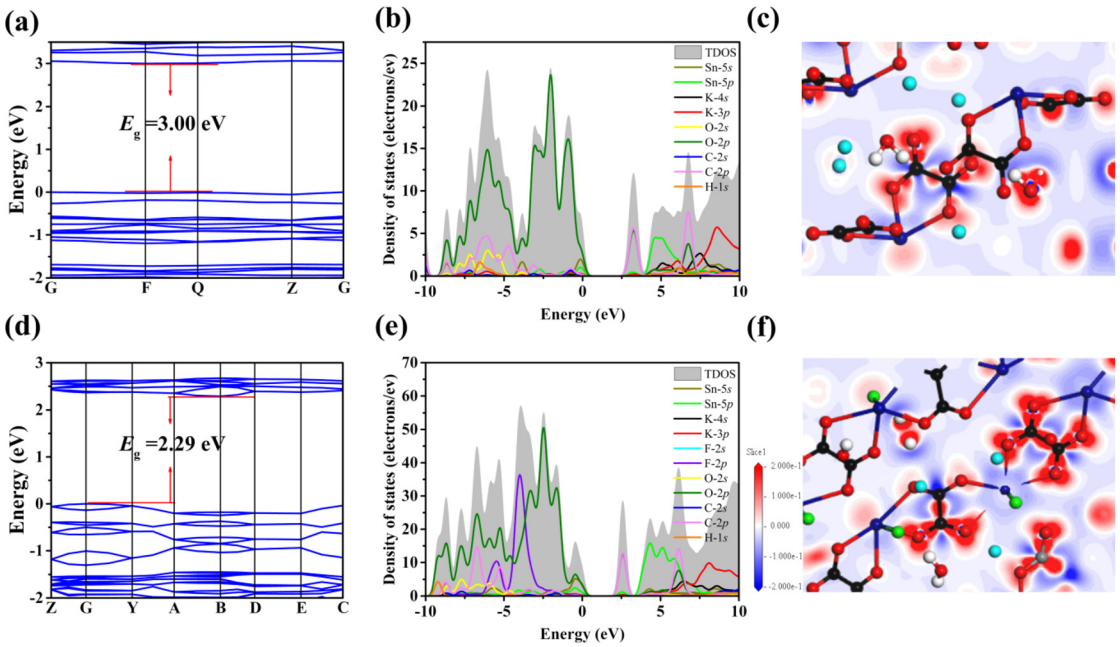

Fig. 5 (a and d) Calculated band structures; (b and e) total and partial density of states; and (c and f) electron density difference maps for $K_2Sn(C_2O_4)_2{\cdot}H_2O$ and $K_2Sn_2(C_2O_4)_2F_2{\cdot}H_2O$.

is charge transfer in the $C_2O_4^{2-}$ planar groups. The result further verified that the large birefringence of the two compounds originated from synergetic interactions of the $C_2O_4^{2-}$ groups and the Sn^{2+} polyhedra.

Conclusions

In brief, $K_2Sn(C_2O_4)_2{\cdot}H_2O$ and $K_2Sn_2(C_2O_4)_2F_2{\cdot}H_2O$ were successfully synthesized, in which Sn^{2+} cations with SCALP and π-conjugated $C_2O_4^{2-}$ anion groups were employed simultaneously to construct a 0D $[Sn(C_2O_4)_2]^{2-}$ anionic structure, and a 1D $[Sn_2(C_2O_4)_2F_2]_\infty^{2-}$ anionic structure, respectively. Significantly, with the increase in dimensionality, the birefringence successfully increases from 0.103@546 nm in $K_2Sn(C_2O_4)_2{\cdot}H_2O$ to 0.301@546 nm in $K_2Sn_2(C_2O_4)_2F_2{\cdot}H_2O$. Detailed structural and property analysis confirmed that the rational molecular engineering of the birefringence-active FMs can induce strong optical anisotropy. The significant experimental results provide the prominent UV birefringent crystals and a meaningful strategy to design novel functional materials with large birefringence.

Author contributions

L. Y. Ren: conceptualization, methodology, investigation, writing – original draft, and writing – review & editing. Y. Q. Zhou and D. J. Gao: data curation. L. L. Cao: formal analysis, project administration, resources, and writing – review & editing. L. H. Cheng: characterization analysis. X. Y. Zhou: investigation. J. X. Ren: theoretical calculation. G. H. Zou and L. Huang: resources and supervision. X. H. Dong: conceptualization and investigation.

Conflicts of interest

There are no conflicts to declare.

Acknowledgements

The authors thank Dr Daichuan Ma at Analytical and Testing Center, Sichuan University for technical help in the Material Studio calculations. This work was supported by the National Natural Science Foundation of China (Grant No. 22201195, 22122106, 22071158, and 21971171), Natural Science Foundation of Sichuan Province (2023NSFSC1066) and the Fundamental Research Funds from Sichuan University (2021SCUNL101).

References

1 X. L. Chen, B. B. Zhang, F. F. Zhang, Y. Wang, M. Zhang, Z. H. Yang, K. R. Poeppelmeier and S. L. Pan, Designing an excellent deep-ultraviolet birefringent material for light polarization, *J. Am. Chem. Soc.*, 2018, **140**, 16311–16319.
2 Z. Y. Xie, L. G. Sun, G. Z. Han and Z. Z. Gu, Optical switching of a birefringent photonic crystal, *Adv. Mater.*, 2008, **20**, 3601–3604.
3 S. J. Han, C. M. Huang, A. Tudi, S. S. Hu, Z. H. Yang and S. L. Pan, *β*-CsB_9O_{14}: a triple-layered borate with edge-

sharing BO_4 tetrahedra exhibiting a short cutoff edge and a large birefringence, *Chem. – Eur. J.*, 2019, **25**, 11614–11619.

4 Z. L. Gao, Q. Wu, X. T. Liu, Y. X. Sun and X. T. Tao, Biaxial crystal α-$BaTeMo_2O_9$: theory study of large birefringence and wide-band polarized prisms design, *Opt. Express*, 2015, **23**, 3851–3860.

5 G. Q. Zhou, J. Xu, X. D. Chen, H. Y. Zhong, S. T. Wang, K. Xu, P. Z. Deng and F. X. Gan, Growth and spectrum of a novel birefringent α-BaB_2O_4 crystal, *J. Cryst. Growth*, 1998, **191**, 517–519.

6 F. Sedlmeir, R. Zeltner, G. Leuchs and H. G. L. Schwefel, High-Q MgF_2 whispering gallery mode resonators for refractometric sensing in aqueous environment, *Opt. Express*, 2014, **22**, 30934–30942.

7 H. T. Luo, T. Tkaczyk, E. L. Dereniak, K. Oka and R. Sampson, High birefringence of the yttrium vanadate crystal in the middle wavelength infrared, *Opt. Lett.*, 2006, **31**, 616–618.

8 G. Ghosh, Dispersion-equation coefficients for the refractive index and birefringence of calcite and quartz crystals, *Opt. Commun.*, 1999, **163**, 95–102.

9 G. Peng, C. S. Lin, H. X. Fan, K. C. Chen, B. X. Li, G. Zhang and N. Ye, $Be_2(BO_3)(IO_3)$: the first anion-mixed van der Waals member in the $KBe_2BO_3F_2$ family with a very strong second harmonic generation response, *Angew. Chem., Int. Ed.*, 2021, **60**, 17415–17418.

10 G. H. Zou, Z. E. Lin, H. M. Zeng, H. Jo, S. J. Lim, T. S. You and K. M. Ok, $Cs_3VO(O_2)_2CO_3$: an exceptionally thermostable carbonatoperoxovanadate with an extremely large second-harmonic generation response, *Chem. Sci.*, 2018, **9**, 8957.

11 G. H. Zou, H. Jo, S. J. Lim, T. S. You and K. M. Ok, $Rb_3VO(O_2)_2CO_3$: a four-in-one carbonatoperoxovanadate exhibiting an extremely strong second-harmonic generation response, *Angew. Chem., Int. Ed.*, 2018, **57**, 8619–8622.

12 R. K. Li and Y. Y. Ma, Chemical engineering of a birefringent crystal transparent in the deep UV range, *CrystEngComm*, 2012, **14**, 5421–5424.

13 W. J. Xie, Z. Fang and J. G. Mao, $Ba_6Zn_6(B_3O_6)_6(B_6O_{12})$: barium zinc borate contains π-conjugated $[B_3O_6]^{3-}$ anions and $[B_6O_{12}]^{6-}$ anion with edge-sharing BO_4 tetrahedra, *Inorg. Chem.*, 2022, **61**, 18260–18266.

14 Z. Li, F. Liang, Y. W. Guo, Z. S. Lin, J. Y. Yao, G. C. Zhang, W. L. Yin, Y. C. Wu and C. T. Chen, $Ba_2M(C_3N_3O_3)_2$ (M=Mg, Ca): potential UV birefringent materials with strengthened optical anisotropy originating from the $(C_3N_3O_3)^{3-}$group, *J. Mater. Chem. C*, 2018, **6**, 12879.

15 L. L. Cao, H. T. Tian, D. H. Lin, C. S. Lin, F. Xu, Y. L. Han, T. Yan, J. D. Chen, B. X. Li, N. Ye and M. Luo, A flexible functional module to regulate ultraviolet optical nonlinearity for achieving a balance between a second-harmonic generation response and birefringence, *Chem. Sci.*, 2022, **13**, 6990.

16 X. P. Shi, W. B. Zhang, W. B. Cai, S. J. Han, Z. H. Yang and S. Pan, $Li_3La_2(BO_3)_3$ and $Li_{1.75}Na_{1.25}La_2(BO_3)_3$: a great enhancement in birefringence induced by optimal arrangement of π-Conjugated $[BO_3]$ Units, *Inorg. Chem.*, 2021, **60**, 12565–12572.

17 W. B. Cai, J. Q. Chen, S. L. Pan and Z. H. Yang, Enhancement of band gap and birefringence induced via π-conjugated chromophore with "tail effect", *Inorg. Chem. Front.*, 2022, **9**, 1224–1232.

18 M. Aibibula, L. Wang and S. Z. Huang, $Rb_3Na(H_2C_3N_3O_3)_4{\cdot}3H_2O$ with Large Birefringence, *ACS Omega*, 2019, **4**, 22197–22202.

19 Z. Z. Zhang, Y. Wang, H. Li, Z. H. Yang and S. L. Pan, $BaB_8O_{12}F_2$: a promising deep-UV birefringent material, *Inorg. Chem. Front.*, 2019, **6**, 546.

20 H. T. Qiu, F. M. Li, C. C. Jin, J. J. Lu, Z. H. Yang, S. L. Pan and M. Mutailipu, $(N_2H_6)[HPO_3F]_2$: maximizing the optical anisotropy of deep-ultraviolet fluorophosphates, *Chem. Commun.*, 2022, **58**, 5594.

21 K. C. Chen, C. S. Lin, J. D. Chen, G. S. Yang, H. T. Tian, M. Luo, T. Yan, Z. G. Hu, J. Y. Wang, Y. C. Wu, N. Ye and G. Peng, Intense d-p hybridization in Nb_3O_{15} tripolymer induced the largest second harmonic generation response and birefringence in germanates, *Angew. Chem., Int. Ed.*, 2023, **62**, e202217039.

22 J. Moon and K. M. Ok, (R)- and (S)-$[C_8H_{10}NO_3]_2[NbOF_5]$: noncentrosymmetric niobium oxyfluorides with large optical anisotropy, *Inorg. Chem. Front.*, 2022, **9**, 2498–2507.

23 M. Aibibula, J. Y. Guo, J. Han, A. Tudi, Z. H. Yang and S. L. Pan, BaTi(BO3)2: an excellent birefringent material with highly coplanar isolated [BO3] groups, *New J. Chem.*, 2021, **45**, 7065.

24 J. Y. Guo, A. Tudi, S. J. Han, Z. H. Yang and S. L. Pan, Sn_2PO_4I: an excellent birefringent material with giant optical anisotropy in non π-conjugated phosphate, *Angew. Chem., Int. Ed.*, 2021, **60**, 24901–24904.

25 Y. L. Deng, L. Huang, X. H. Dong, L. Wang, K. M. Ok, H. M. Zeng, Z. E. Lin and G. H. Zou, $K_2Sb(P_2O_7)F$: cairo pentagonal layer with bifunctional genes reveal optical performance, *Angew. Chem., Int. Ed.*, 2020, **59**, 21151–21156.

26 Y. C. Liu, X. M. Liu, S. Liu, Q. R. Ding, Y. Q. Li, L. N. Li, S. G. Zhao, Z. S. Lin, J. H. Luo and M. C. Hong, An unprecedented antimony(III) borate with strong linear and nonlinear optical responses, *Angew. Chem., Int. Ed.*, 2020, **59**, 7793–7796.

27 J. Chen, C. L. Hu and J. G. Mao, $LiGaF_2(IO_3)_2$: a mixed-metal gallium iodate-fluoride with large birefringence and wide band gap, *Sci. China Mater.*, 2021, **64**, 400–407.

28 S. Y. Niu, G. Joe, H. Zhao, Y. C. Zhou, T. Orvis, H. Huyan, J. Salman, K. Mahalingam, B. Urwin, J. B. Wu, Y. Liu, T. E. Tiwald, S. B. Cronin, B. M. Howe, M. Mecklenburg, R. Haiges, D. J. Singh, H. Wang, M. A. Kats and J. Ravichandran, Giant optical anisotropy in a quasi-one dimensional crysta, *Nat. Photonics*, 2018, **12**, 392–396.

29 P. F. Gong, S. Z. Zhang, G. M. Song, X. M. Liu and Z. S. Lin, An unprecedented planar π-conjugated $[B_2P_5]^{5-}$group with ultra-large birefringence and nonlinearity: an ab initio study, *Chem. Commun.*, 2020, **56**, 643.

30 D. Zhang, Q. Wang, L. Y. Ren, L. L. Cao, L. Huang, D. J. Gao, J. Bi and G. H. Zou, Sharp enhancement of birefringence in antimony oxalates achieved by the cation–-anion synergetic interaction strategy, *Inorg. Chem.*, 2022, **61**, 12481–12488.

31 G. H. Zou, C. S. Lin, H. Jo, G. Nam, T. S. You and K. M. Ok, Pb_2BO_3Cl: a tailor-made polar lead borate chloride with very strong second harmonic generation, *Angew. Chem., Int. Ed.*, 2016, **55**, 12078–12082.

32 Y. Long, X. H. Dong, H. M. Zeng, Z. E. Lin and G. H. Zou, Layered perovskite-like nitrate $Cs_2Pb(NO_3)_2Br_2$ as a multifunctional optical material, *Inorg. Chem.*, 2022, **61**, 4184–4192.

33 Y. X. Chen, Z. X. Chen, Y. Zhou, Y. Q. Li, Y. C. Liu, Q. R. Ding, X. Chen, S. G. Zhao and J. H. Luo, An antimony (III) fluoride oxalate with large birefringence, *Chem. – Eur. J.*, 2021, **27**, 4557–4560.

34 Y. W. Ge, Q. Wang, F. Yang, L. Huang, D. J. Gao, J. Bi and G. H. Zou, Tin chloride sulfates $A_3Sn_2(SO_4)_{3-x}Cl_{1+2x}$ (A=K, Rb, Cs; x=0, 1) as multifunctional optical materials, *Inorg. Chem.*, 2021, **60**, 8322–8330.

35 H. X. Qi, H. Jo, X. L. Chen, J. Hong and K. M. Ok, Second-harmonic generation and photoluminescence properties of Sn(II)- and Bi(III)-based lone pair cation-pyridine dicarboxylate coordination compounds, *Inorg. Chem.*, 2020, **59**, 11554–11561.

36 R. A. Li, Z. Y. Zhou, Y. K. Lian, F. Jia, X. X. Jiang, M. C. Tang, L. M. Wu, J. L. Sun and L. Chen, A_2SnS_5: a structural incommensurate modulation exhibiting strong second-harmonic generation and a high laser-induced damage threshold (A=Ba, Sr), *Angew. Chem., Int. Ed.*, 2020, **59**, 11861–11865.

37 J. Y. Guo, A. Tudi, S. J. Han, Z. H. Yang and S. L. Pan, $Sn_2B_5O_9Cl$: a material with large birefringence enhancement activated prepared via alkaline-earth-metal substitution by Tin, *Angew. Chem., Int. Ed.*, 2019, **58**, 17675–17678.

38 J. Y. Guo, A. Tudi, S. J. Han, Z. H. Yang and S. L. Pan, α-SnF_2: a UV birefringent material with large birefringence and easy crystal growth, *Angew. Chem., Int. Ed.*, 2021, **60**, 3540–3544.

39 M. J. Schäfer, S. G. Jantz, F. Pielnhofer and H. A. Höppe, The very first normal-pressure tin borate $Sn_3B_4O_9$, and the intermediate $Sn_2[B_7O_{12}]F$, *Dalton Trans.*, 2019, **48**, 10398.

40 T. H. Tong, W. Y. Zhang, Z. H. Yang and S. L. Pan, Series of crystals with giant optical anisotropy: a targeted strategic research, *Angew. Chem., Int. Ed.*, 2021, **60**, 1332–1338.

41 D. Zhang, Q. Wang, T. Zheng, L. L. Cao, K. M. Ok, D. J. Gao, J. Bi, L. Huang and G. H. Zou, Cation-anion synergetic interactions achieving tunable birefringence in quasi-one-dimensional antimony(III) fluoride oxalates, *Sci. China Mater.*, 2022, **65**, 3115–3124.

42 G. M. Sheldrick, A short history of SHELX, *Acta Crystallogr., Sect. A: Found. Crystallogr.*, 2008, **64**, 112–122.

43 A. L. Spek, Single-crystal structure validation with the program PLATON, *J. Appl. Crystallogr.*, 2003, **36**, 7–13.

44 S. J. Clark, M. D. Segall, C. J. Pickard, P. J. Hasnip, M. I. J. Probert, K. Refson and M. C. Payne, First principles methods using CASTEP, *Z. Kristallogr. - Cryst. Mater.*, 2005, **220**, 567–570.

45 M. D. Segall, P. J. D. Lindan, M. J. Probert, C. J. Pickard, P. J. Hasnip, S. J. Clark and M. C. Payne, First-principles simulation: ideas, illustrations and the CASTEP code, *J. Phys.: Condens. Matter*, 2002, **14**, 2717–2744.

46 D. Vanderbilt, Soft self-consistent pseudopotentials in a generalized eigenvalue formalism, *Phys. Rev. B: Condens. Matter Mater. Phys.*, 1990, **41**, 7892.

47 K. Kobayashi, Norm-conserving pseudopotential database (NCPS97), *Comput. Mater. Sci.*, 1999, **14**, 72–76.

48 A. D. Christie, R. A. Howie and W. Moser, Tin(II) oxalate structures, *Inorg. Chim. Acta*, 1979, **36**, L447–L448.

49 L. D. Luan, J. Li, C. Chen, Z. E. Lin and H. Huang, Solvent-free synthesis of crystalline metal phosphate oxalates with a (4,6)-connected fsh topology, *Inorg. Chem.*, 2015, **54**, 9387–9389.

50 Y. V. Kokunov, D. G. Detkov, Y. E. Gorbunova, M. M. Ershova, Y. N. Mikhailov and Y. A. Buslaev, Crystal structure of $(NH_4)_2Sn_2F_4(NO_3)_2$: the first example of dimeric $[Sn_2F_4E_2]$ complexes in Tin(II) fluorides, *Dokl. Chem.*, 2001, **378**, 135–138.

51 Y. V. Kokunov, D. G. Detkov, Y. E. Gorbunova, M. M. Ershova and Y. N. Mikhailov, Synthesis and crystal structure of calcium trifluorostannate(II), *Dokl. Chem.*, 2001, **376**, 52–54.

52 D. E. Zelmon, D. L. Small and D. Jundt, Infrared corrected Sellmeier coefficients for congruently grown lithium niobate and 5 mol% magnesium oxide–doped lithium niobate, *J. Opt. Soc. Am.*, 1997, **14**, 3319–3322.

53 J. R. Devore, Refractive indices of rutile and sphalerite, *J. Opt. Soc. Am.*, 1951, **41**, 416–419.

54 Y. X. Chen, T. T. Zhu, Z. Y. Xiong, Y. Zhou, Y. Q. Li, Q. R. Ding, Y. C. Liu, X. Chen, S. G. Zhao and J. H. Luo, An organic-inorganic hybrid birefringent material with diverse functional groups, *Chem. Commun.*, 2021, **57**, 6668.

55 R. E. Dinnebier, S. Vensky, M. Jansen and J. C. Hanson, Crystal structures and topological aspects of the high-temperature phases and decomposition products of the alkali-metal oxalates $M_2[C_2O_4]$ (M=K, Rb, Cs), *Chem. – Eur. J.*, 2005, **11**, 1119–1129.

56 D. Zhang, Q. Wang, H. Luo, L. L. Cao, X. H. Dong, L. Huang, D. J. Gao and G. H. Zou, Deep eutectic solvents synthesis of $A_2Sb(C_2O_4)Cl_3$ (A=NH4, K, Rb) with superior optical performance, *Adv. Opt. Mater.*, 2023, **11**, 2202874.

57 J. L. Song, C. L. Hu, X. Xu, F. Kong and J. G. Mao, A facile synthetic route to a new SHG material with two types of parallel π-conjugated planar triangular units, *Angew. Chem., Int. Ed.*, 2015, **54**, 3679–3682.

